YALE PEABODY MUSEUM

JOURNAL OF MARINE RESEARCH

The *Journal of Marine Research,* one of the oldest journals in American marine science, published important peer-reviewed original research on a broad array of topics in physical, biological, and chemical oceanography vital to the academic oceanographic community in the long and rich tradition of the Sears Foundation for Marine Research at Yale University.

An archive of all issues from 1937 to 2021 (Volume 1–79) are available through EliScholar, a digital platform for scholarly publishing provided by Yale University Library at https://elischolar.library.yale.edu/.

Requests for permission to clear rights for use of this content should be directed to the authors, their estates, or other representatives. The *Journal of Marine Research* has no contact information beyond the affiliations listed in the published articles. We ask that you provide attribution to the *Journal of Marine Research.*

Yale University provides access to these materials for educational and research purposes only. Copyright or other proprietary rights to content contained in this document may be held by individuals or entities other than, or in addition to, Yale University. You are solely responsible for determining the ownership of the copyright, and for obtaining permission for your intended use. Yale University makes no warranty that your distribution, reproduction, or other use of these materials will not infringe the rights of third parties.

Sensitivity of the meridional transport in a 1.5-layer ocean model to localized mass sources

by C. Herbaut[1,2], J. Sirven[1] and J. Deshayes[2]

ABSTRACT

The response of a 1.5-layer ocean model forced by localized stochastic mass sources is studied. The focus is on the sensitivity of the spectral characteristics of the meridional transport to the location and the extent of the source region. In all the experiments, performed in hemispheric and interhemispheric basins, the spectra show a peak at interannual time scale revealing the existence of an oscillation. The period of the oscillation is defined by the zonal extent of the forcing, whereas its amplitude is affected by its location. When the source region is located in the northwestern corner of the basin, the peak emerges clearly on the spectrum of the meridional transport, whereas it is strongly reduced when the source region is located in open ocean. The extension to an inter-hemispheric basin increases the energy at the period of the oscillation, but the introduction of the equatorial dynamics does not affect the spectral characteristics of the response for periods longer than 1 year.

1. Introduction

Observations (Kushnir, 1994) and numerical models (Hakkinen, 2001) have shown that the Atlantic Ocean exhibits variability at multidecadal timescale which might be linked to the meridional overturning circulation (hereafter MOC). However, the observations are too sparse to fully document the variability of the MOC and to understand its mechanism. Numerical models are therefore useful to complement them. Timmerman and Latif (1998), using a coarse resolution coupled ocean-atmosphere model, suggested that the MOC variability reflected an active coupling between atmosphere and ocean, whereas it primarily resulted from the ocean response to stochastic atmospheric forcing via surface heat exchanges in the GFDL coupled model (Delworth and Greatbatch, 2000). Bentsen *et al.* (2004) similarly found that the MOC variability is forced by the atmosphere through deep water formation in the Bergen Climate Model. Our paper focuses on the oceanic aspect of this mechanism: using an idealized ocean model, we examine how the variability of the buoyancy forcing can affect the time evolution of the MOC.

In a work based on a two-layer model, Kawase (1987) investigated the adjustment of the deep layer to a change in deep water formation. The formation of deep water was

1. Université Pierre et Marie Curie, Tour 45, étage 4, CC 100 4 place Jussieu, 75252 PARIS CEDEX 05, France.
2. Corresponding author. *email: christophe.herbaut@lodyc.jussieu.fr*

parameterized by a mass exchange between the layers while a damping term simulated the role of diffusion. The adjustment of the model was achieved through Kelvin waves which propagated along the western boundary from the mass source, in the northwestern corner of the basin, to the equator. The signal was then transmitted by equatorial Kelvin waves to the eastern boundary, where Rossby waves were radiated westward, preventing variations with latitude of the thermocline depth along the eastern boundary, as discussed by Johnson and Marshall (2002) (hereafter JM). For a weak damping, the mechanism leads to the steady state of Stommel and Arons (1960). Using a 1.5-layer reduced gravity model, Huang *et al.* (2000) studied the adjustment of the global ocean to a sudden change in deep water formation. For a reasonable damping value and a formation rate of 10 Sv in the northern Atlantic, the authors found that the thermocline depth adjusted on centennial time scale with respective variations of 100 and 50 m in the Atlantic and Pacific oceans. Using a similar model, but forced by a meridional mass transport at the northern boundary, JM investigated the adjustment of the meridional transport on the basin scale. They showed that, in an interhemispheric basin, the response in the southern hemisphere represents only a small fraction of the changes observed in the northern hemisphere. The periodic forcing case was discussed by Johnson and Marshall (2004), while Deshayes and Frankignoul (2005) (hereafter DF) considered the model response to stochastic fluctuations in the transport at the northern boundary. The latter showed that most of the variance of the meridional transport is found at low frequencies, but without showing any preferred time scale.

None of these studies considered the possible influence of the nature of the forcing (by downwelling in Kawase (1987), or by horizontal mass inflow through boundary in JM or DF). Yang and Price (2000) investigated this issue with theoretical and numerical studies. The 1 Sv mass flux was identical in both cases (downwelling and horizontal mass inflow through boundary) but, as the potential vorticity flux differed, the solution could vary, depending on the location of the forcing. When the source was located in the northwestern corner of the basin, the steady state solution was very similar in both cases. When the source was located along the eastern boundary, the circulation generated south of the source by the local downwelling became weaker than that generated by a mass inflow, and a β-plume recirculation (Pedlosky, 1996; Spall, 2000) characterized by a strong zonal circulation at the latitude of the downwelling source was formed.

Using a a 1.5-layer reduced gravity model, we study the response of the total meridional mass transport, which represents the upper branch of the MOC in this type of model, to stochastic fluctuations of the deep water formation. The water formation is parameterized by a localized water mass exchange as in Kawase (1987) and Huang *et al.* (2000). Following Yang and Price (2000), the influence of the location of the source is studied and the impact of its meridional and zonal extension is also analysed. Finally, the model domain is extended to the southern hemisphere to investigate the importance of the "equatorial buffer" pointed at by JM.

2. Model and experimental set-up

The model is a shallow water reduced gravity model with one active layer of mean thickness of 800 m above an infinite layer at rest. The model predicts the thickness h_1 and the velocity $\mathbf{v}_1$ of the active layer that obeys:

$$\frac{\partial \mathbf{v}_1}{\partial t} + (curl.\mathbf{v}_1 + f)\mathbf{k} \wedge \mathbf{v}_1 = -\mathbf{grad}(b_1 h_1 + \mathbf{v}_1^2/2) + \nu\nabla^2\mathbf{v}_1 \tag{1}$$

$$\frac{\partial h_1}{\partial t} + \mathrm{div}(h_1\mathbf{v}_1) = w_e \tag{2}$$

where $b_1 = 0.08$ m s^{-2}, the viscosity coefficient ν is equal to 100 m^2 s^{-1}, $\mathbf{k}$ is a vector normal to the Earth's surface, and w_e represents a sink or source of mass.

The equations are solved on the sphere and discretized with a finite difference scheme on a C-grid, whose spatial resolution is 1/5°. The numerical scheme preserves enstrophy. No slip boundary conditions are applied and the gradient of h_1 is assumed to be tangent to the boundary (no normal flow boundary condition). The domain extends from 0 to 60E in all the experiments, but its latitudinal extent is either 15N-50N or 40S-50N. Sensitivity experiments with various locations and zonal extents of the source region have been performed. JM and DF developed their theory in a linear framework, whereas we have used a nonlinear model. In order to estimate the impact of the nonlinear terms, an experiment with a linear version of the model is made. This linear model solves the following equations:

$$\frac{\partial \mathbf{v}_1}{\partial t} + f\mathbf{k} \wedge \mathbf{v}_1 = -\mathbf{grad}(b_1 h_1) + \nu\nabla^2\mathbf{v}_1 \tag{3}$$

$$\frac{\partial h_1}{\partial t} + \mathrm{div}(H_1\mathbf{v}_1) = w_e. \tag{4}$$

In all the experiments, the time series of the forcing is a random process with a zero mean and a white spectrum. The standard deviation of the mass exchange is set to 3.5 Sv; this value is in agreement with the fluctuations of the Labrador Sea Water formation rate observed by Rhein *et al.* (2002). Indeed, these authors estimated a rate of about 10 Sv in 1988–1994, but of only 2 Sv in 1995–1997. Table 1 summarizes the set-up of all the experiments.

3. Results

a. The forcing is close to the northwestern coast

In experiment $1\mathrm{H}_{a1}$, the forcing is localized in the northwestern corner of the domain, between 0 and 6E, and 43 and 50N. The source region extends over a $6° \times 7°$ area, which is large compared to the extension of convection sites in the ocean. However, the downwelling regions are distinguishable from convective mixing regions (Marotzke and Scott, 1999) and can have a larger extent. As noticed by Yang and Price (2000), the currents (especially along the western boundary) are much greater near the source. Therefore two separate analyses have been done, one for the forcing area and another for the rest of the basin.

Table 1. Set-up of the experiments.

Experiment	Domain	Source region: meridional extent	Source region: zonal extent	Model
$1H_{a1}$	15-50N 0-60E	43-50N	0-6E	nonlinear
$1H_{a2}$	15-50N 0-60E	43-50N	0-12E	nonlinear
$1H_{b1}$	15-50N 0-60E	38-45N	30-36E	nonlinear
$1H_{b2}$	15-50N 0-60E	38-45N	30-42E	nonlinear
$1H_{b3}$	15-50N 0-60E	38-45N	30-48E	nonlinear
$1H_{b4}$	15-50N 0-60E	38-45N	30-54E	nonlinear
$1H_{b5}$	15-50N 0-60E	38-45N	0-6E	nonlinear
$1H_{b6}$	15-50N 0-60E	38-45N	10-16E	nonlinear
$1H_{b7}$	15-50N 0-60E	38-45N	50-56E	nonlinear
$1H_{b8}$	15-50N 0-60E	44-45N	30-36E	nonlinear
$2H_a$	40S-50N 0-60E	43-50N	30-36E	nonlinear
$2H_{al}$	40S-50N 0-60E	43-50N	30-36E	linear
$2H_b$	2S-50N 0-60E	43-50N	30-36E	nonlinear

Figure 1 shows the first three EOFs of the meridional velocity computed over the source region. The first EOF, which represents about 60% of the total variance, displays a dipole with a positive sign in the source region and a negative sign in the western boundary. This pattern looks like the intense recirculation near the western boundary described by Yang and Price (2000). This recirculation, whose contribution is essential to the potential vorticity budget of the basin, is a characteristic feature of the circulation of a reduced-gravity model forced by a downwelling source (Yang and Price, 2000). The spectrum of the associated principal component (hereafter PC) shows the existence of a dominant timescale of 3.5–4 years. The second and third EOFs show wave-like patterns of higher modes while the corresponding PCs have dominant periods of respectively 1 and 2 years.

Over the interior basin, the first two EOFs of the meridional velocity represent each one about 16% of the variance and their patterns suggest Rossby wave fronts (Fig. 2). PC1 is strongly correlated with PC2 at a lag of +1 year, indicating a westward propagation. Rossby waves propagation is also apparent on the time-longitude diagram of the meridional velocity at 30N (Fig. 3). The timescale of propagation deduced from this diagram agrees with the velocity of baroclinic Rossby waves (computed with the reduced gravity of our model). The autocorrelations of PC1 and PC2 show the existence of a damped oscillation with a 3.5–4 year period.

When the zonal extent of the forcing zone is doubled without changing the standard deviation of the mass exchange (exp. $1H_{a2}$), the first two EOFs (PCs) display a signal whose wavelength (period) is about twice as long as in $1H_{a1}$, suggesting that the period of the oscillation might be set by the zonal extent of the source region.

Figure 4 displays the spectrum of the total meridional transport at various latitudes. It has less variance at low latitudes than at high latitudes for periods longer than 2 years, and it is independent of latitude at high frequency. It also exhibits a maximum of variance for periods
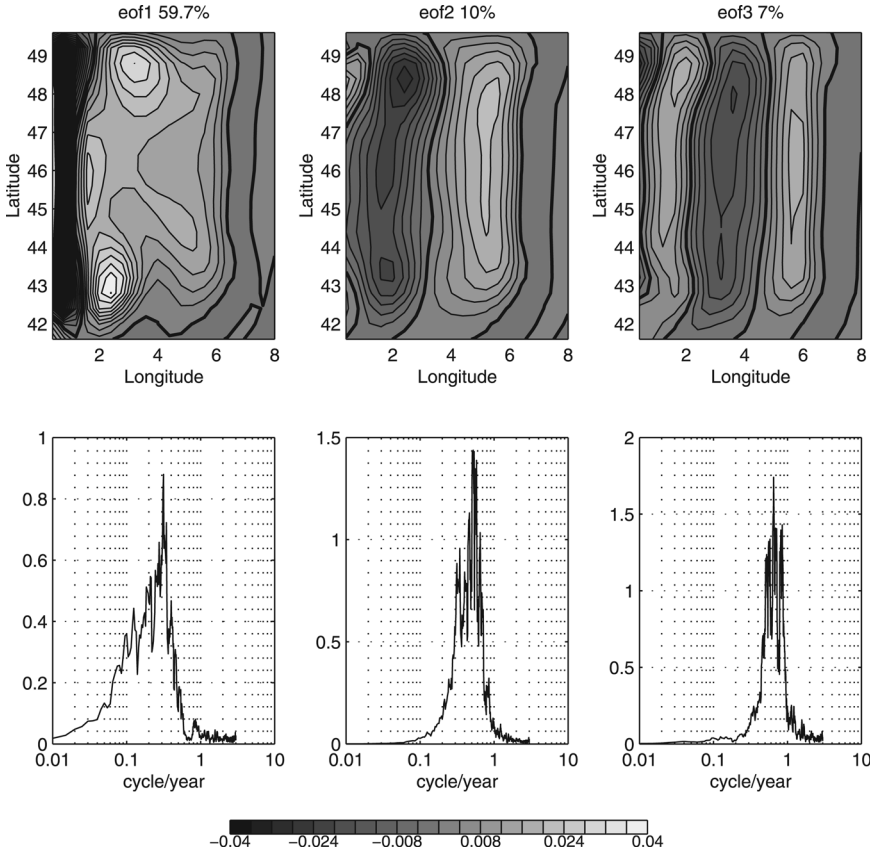
Figure 1. First three EOFs of the meridional velocity in experiment $1H_{a1}$ (in m s^{-1}) in the source region (top) and the variance conserving spectra of the associated PCs (bottom).

ranging from 3 to 4 years (significative at 95% confidence level on a power spectrum), which is associated to the previously described oscillation. A significant part of the variance is also found at periods shorter than 1 year. A large part of this high frequency energy is generated in the forcing area by the excitation of Rossby waves of short wavelength, the instability of the current and the formation of eddies, and is transmitted to the western boundary current by the Kelvin waves.

DF explained the southward decrease of the total transport by the increasing influence of the interior transport as the frequency decreases. The interior transport, which is generated by the propagation of the Rossby waves, adjusts when the waves reach the western boundary. As the velocity of the Rossby waves decreases with latitude, the timescale of the adjustment depends on latitude: at high latitudes it occurs at longer timescale and thus lower frequencies than at low latitudes. On the other hand, when the Rossby waves reach the
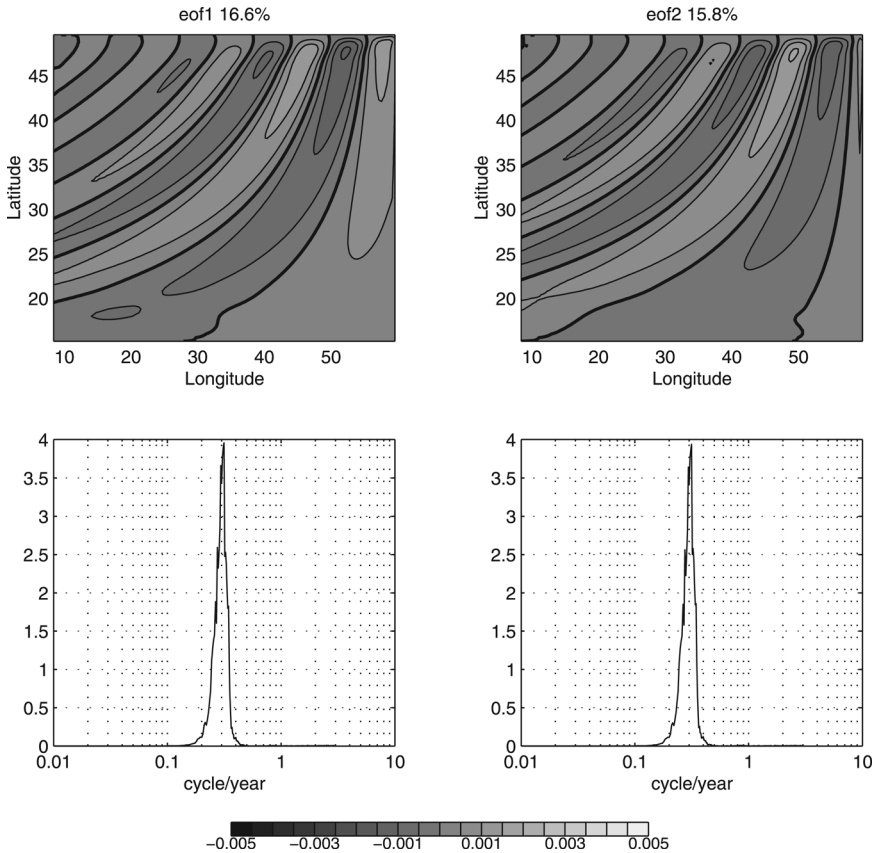
Figure 2. First (top left) and second (top right) EOFs of the meridional velocity in experiment $1H_{a1}$ (in m s^{-1}) and the variance conserving spectra of the associated PCs (bottom).

western boundary, the transport in the western boundary is altered leading to a decrease of the total meridional transport. Therefore, at high frequency, the interior transport is adjusted and the total transport is weak at low latitudes, while the total transport remains high at higher latitudes.

b. The forcing is away from the boundaries

In experiment $1H_{b1}$, the forcing is localized away from the boundaries, between 30-36E, and 38-45N. The first two EOFs of the meridional velocity show that waves of about 3.5 year period propagate from the forcing zone to the western boundary between 35N and 45N (Fig. 5). The patterns of the first two EOFs south of the source region (not shown) are similar to those obtained in experiment $1H_{a1}$, and the spectra of the associated PCs are still dominated by a 3.5 year peak.
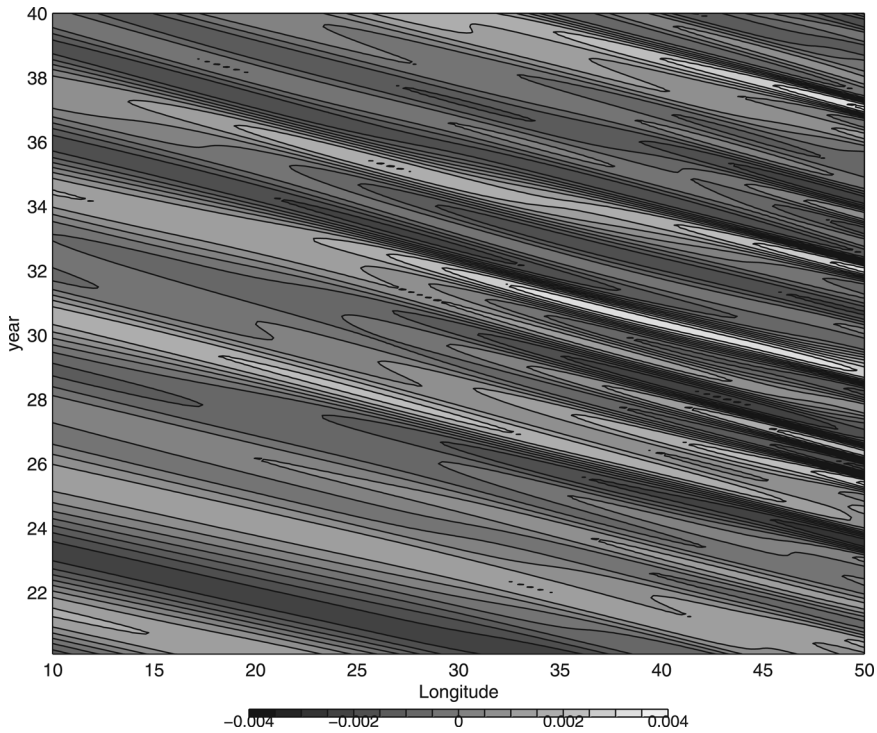
Figure 3. Time-longitude diagram of the meridional velocity at 30N in experiment $1H_{a1}$ (m s^{-1}).

Sensitivity experiments with a zonal extent of the forcing zone mutiplied by 2, 3 and 4 has been performed (exp. $1H_{b2}$, $1H_{b3}$, $1H_{b4}$), and, as for $1H_{a1}$, an EOF analysis of the meridional velocity has been performed. On Figure 6, the spectra of PC1 for these experiments show that the timescale of the response increases linearly with the zonal extent of the forcing area. This timescale corresponds to the half period of a first baroclinic Rossby wave whose half wave length is equal to the zonal extent of the forcing area (about 1.5 years for the half period at 45°N, when the zonal extent of the source region is 6° and using the reduced gravity of the model to compute the Rossby wave velocity). The oscillation is thus set in the source region and transmitted to the western boundary through Rossby waves, then into the whole basin via coastal Kelvin and Rossby waves.

Figure 7 displays the spectrum of the total meridional transport at various latitudes in $1H_{b1}$. The energy at periods shorter than 5 years is much smaller than in experiment $1H_{a1}$. This is associated with a 30% decrease of the total meridional transport. To determine the origin of this decrease, a series of experiments is performed to test the evolution of the response in function of the location of the source region with respect ot the western boundary. In these experiments the source region is successively located at 0-6E (exp. $1H_{b5}$), 10-16E (exp. $1H_{b6}$), 50-56E (exp. $1H_{b7}$). The spectra of the total meridional transport at 30N
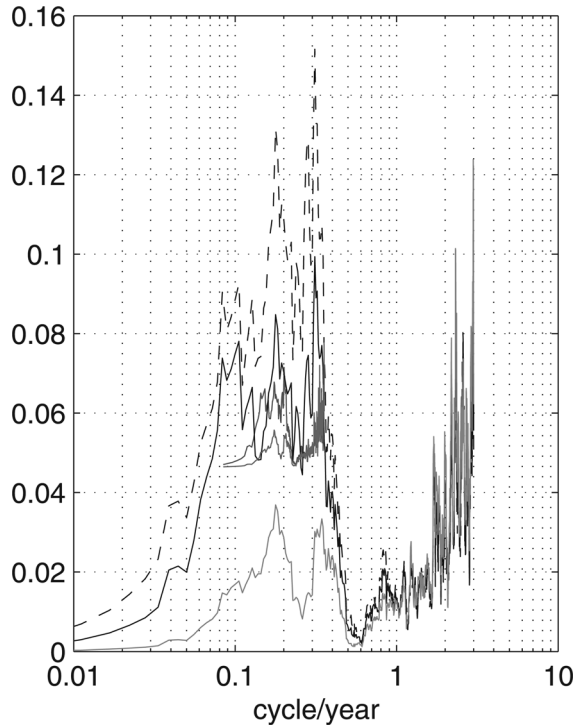
Figure 4. Spectrum of the total transport in experiment $1H_{a1}$ at 40N (dashed line), 30N (solid dark line), 20N (light line).

computed in the 4 experiments and displayed on Figure 8 show a decrease of the meridional transport as the source region is located further off shore.

Indeed, the energy is instantaneously transmitted along the western boundary by Kelvin waves in experiments $1H_{a1}$ and $1H_{b5}$ while it reaches the western boundary thanks to the westward propagation of Rossby waves in experiment $1H_{b1}$, $1H_{b6}$ and $1H_{b7}$. As the dissipation is scale selective in our model, the Rossby waves of period shorter than 1 year are strongly damped when traveling across the basin whereas Rossby waves of longer periods are only weakly dissipated. Thus the dissipation can explain the decrease of energy only at periods shorter than 1 year.

The pattern of the perturbation in experiments $1H_{b1}$, $1H_{b6}$ and $1H_{b7}$ is distorted as it propagates westward (see for example Fig. 5 for exp. $1H_{b1}$): the southern edge moves faster than the northern one, and the wavelength of the wave is longer at the southern limit of the forcing area. Therefore, at each latitude, the perturbations generated at the western boundary will have slightly different periods and will not oscillate in phase. The interferences between these signals would tend to reduce the amplitude of the oscillation along the western boundary at the latitudes of the forcing zone, from where the signal is
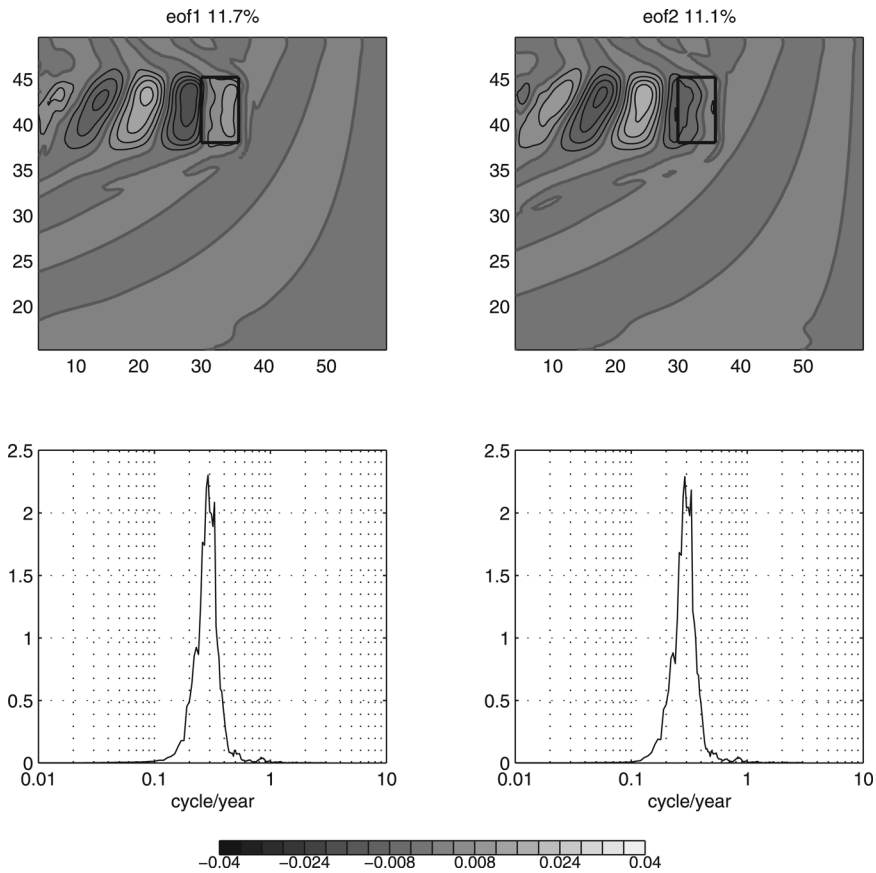
Figure 5. EOFs of the meridional velocity in experiment $1H_{b1}$ (in m s^{-1}) and the variance conserving spectra of the associated PCs (bottom). The box indicates the position of the source region.

transmitted to the whole basin. When the forcing area is close to the coast, as in experiment $1H_{a1}$ the phase lags are reduced, inducing a weaker damping.

To confirm this hypothesis, we performed an experiment ($1H_{b8}$) similar to $1H_{b1}$, except that the meridional extent of the source region is reduced to 1°. The southern and northern edges of the perturbation propagating from the source region travel with a quasi identical velocity (not shown), and as expected, the 3.5 year peak again emerges clearly and represents a maximum of variance in the spectrum of the total transport (not shown).

The influence of the variation of the Rossby wave velocity on the amplitude of the response was already noticed by Primeau (2002), who showed that the resonance of the basin modes is reduced when the lines of constant phase of the long Rossby waves, which are essential for the set-up of the modes, are not parallel to the western boundary.
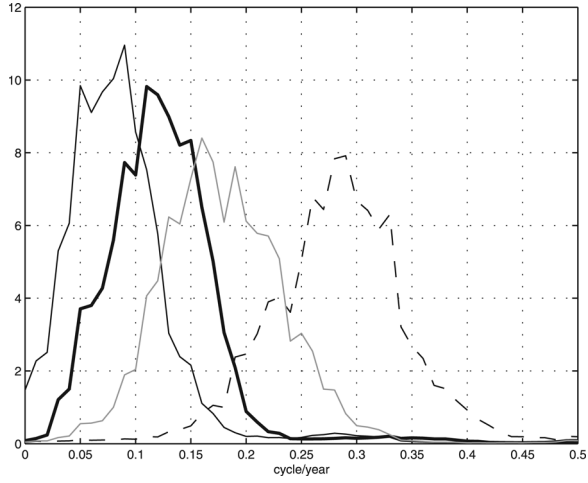
Figure 6. Spectrum of the first principal component of the meridional velocity in experiments $1H_{b1}$ (dashed line), $1H_{b2}$ (light line), $1H_{b3}$ (bold line), $1H_{b4}$ (thin dark line).
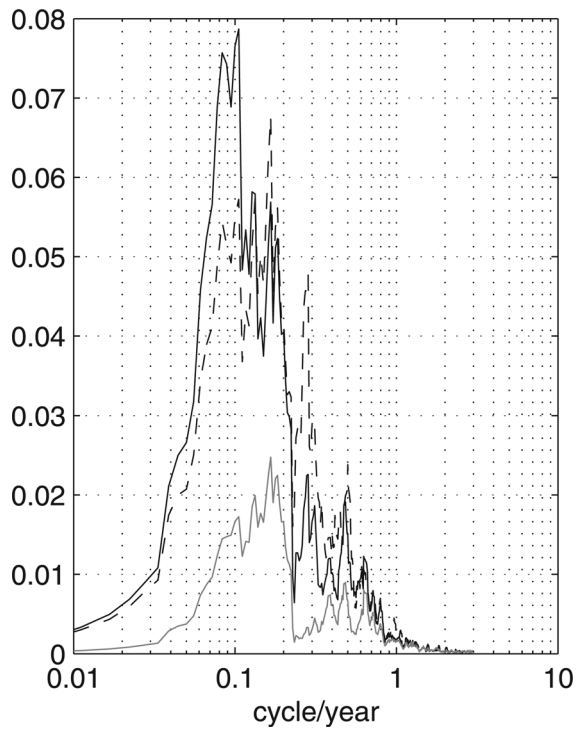

Figure 7. Spectrum of the total transport in experiment $1H_{b1}$ at 40N (dashed line), 30N (dark line), 20N (light line) .
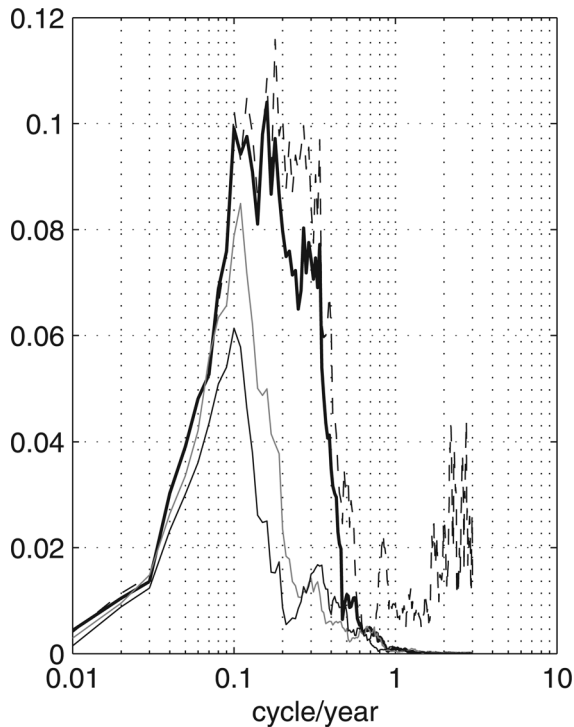
Figure 8. Spectrum of the total transport at 30N in experiments $1H_{b5}$ (dashed line), $1H_{b6}$ (bold line), $1H_{b7}$ (thin dark line) $1H_{b1}$ (light line).

c. Response in an interhemispheric basin

The model is now extended to the southern hemisphere (experiment $2H_a$), but the forcing remains the same as in exp. $1H_{a1}$. The perturbations created in the forcing area are now transmitted to the eastern boundary by equatorial Kelvin waves, which then excite coastal Kelvin waves propagating poleward in the northern and southern hemispheres.

As in $1H_{a1}$, the amplitude of the depth perturbation linked with the Kelvin fronts propagating along the western boundary decreases equatorward. However, as the Kelvin fronts now propagate down to the equator, the amplitude of the thermocline depth variations transmitted to the eastern boundary undergoes a stronger decrease than in experiment $1H_{a1}$. Indeed the conservation of the energy flux of the Kelvin waves implies that the amplitude of the thermocline depth variations decreases as the square root of the Coriolis parameter (cf Gill, 1982, p. 380, and JM who also emphasized this decrease). Thus, the Rossby waves generated at the eastern boundary now have a lower amplitude and the interior transport has less influence than in experiment $1H_{a1}$. This is illustrated on Figure 9 which displays the spectrum of the total meridional transport. The decadal periods represent a smaller part of variance because of the smaller influence of the Rossby waves which (for the slowest
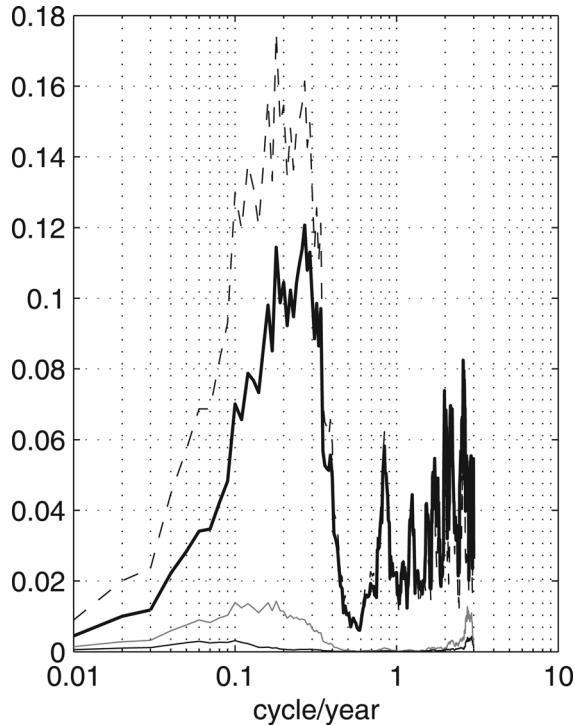
Figure 9. Spectrum of the total transport in experiment $2H_a$ at 30N (dashed line), 10N (bold line), 10S (light line), 20S (thin dark line).

ones) tend to bring energy at decadal periods, and the equatorward decrease is reduced. As a consequence, the 3.5–4 year peak is more pronounced than in experiment $1H_{a1}$.

To estimate the influence of the dynamics of the southern hemisphere on the meridional transport in the northern hemisphere, an experiment ($2H_b$), where the domain extends from 2S to 50N, was performed. The spectra of the total meridional transports in $2H_a$ and $2H_b$ are very similar suggesting that the dynamics in the southern hemisphere does not impact on the northern hemisphere. This experiment also stresses that the changes between $1H_{a1}$ and $2H_a$ are mainly due to the dynamics implied by the equatorward extension of the northern hemisphere.

Even if the spectra of the meridional transport are different, the results from this experiment are qualitatively similar to those obtained by DF: in the northern hemisphere the total transport decreases with latitudes at low frequencies and is much stronger than that in the southern hemisphere, where it strongly decreases poleward (Fig. 9).

Finally, we have performed an experiment (exp. $2H_{al}$) with a similar set-up to experiment $2H_a$, but with a linear version of the model. The response is quasi identical to that of experiment $2H_a$ suggesting that the linear theory developed by JM and DF mainly applies

to our experiments and that the differences in the spectra of the meridional transport between our study and that of DF are due to the forcing and the better representation of the equatorial wave dynamics.

4. Discussion and conclusion

The response of a 1.5-layer reduced gravity model to a localized mass source is studied. When a stochastic forcing is applied, an interannual oscillation emerges over the whole basin. The zonal extent of the source region defines the period of the oscillation and the localization affects its intensity. Indeed, a wave, whose frequency is determined by the length of the forcing area, is generated in the source region. It is then transmitted along the western and southern boundaries by Kelvin waves, then from the eastern boundary to the whole domain via long Rossby waves. Using an analytical model opened at the western boundary and forced by atmospheric patterns, Jin (1997) already suggested that peaks whose location in the frequency domain depends on the wavelength of the forcing, can emerge in the spectrum of the meridional transport.

When the forcing area is located away from the boundaries, the total meridional transport decreases. This decrease which is all the more important since the source region is moved farther east, can reach 30% for a source region located at mid-basin. Rahmstorf (1995) mentioned that the meridional overturning is sensitive to the location of deep convection: the addition of grid-point fresh water anomalies in a forced ocean model of coarse resolution modifies the convection patterns and leads to different overturning rate. In our model, when the source region is located off the boundary, the perturbations of the thermocline depth, propagating from the forcing area, display a phase lag due to the variation of the velocity of the first baroclinic Rossby waves with latitude. As mentioned by Primeau (2002), at the western boundary, the interferences between these signals are thus less constructive, and the amplitude of the response is reduced. When, the latitudinal extent of the source region is reduced, the interferences are attenuated and the peak associated with the oscillation emerges more clearly on the spectrum of the meridional transport.

The extension from a mid latitude basin to an interhemispheric basin increases the energy of the meridional transport at the period of the oscillation (generated by the forcing), as the interior transport is strongly weakened. Indeed, the amplitude of the thermocline depth perturbations, induced by the Kelvin waves propagation along the western boundary, varies as the square root of the Coriolis parameter, and becomes very weak close to the equator. The signal transmitted to the eastern boundary is consequently very weak and the interior dynamics is strongly weakened.

In a resembling study, save that the model was linear and forced by an horizontal transport through the northern boundary, DF already noticed that the meridional transport was mainly concentrated in the western boundary. However, these authors found that the spectrum of the meridional transport at 40N exhibited a -2 slope for periods between 1 to 50 yr, whereas in our model it is characterized by a peak in the 2–10 year period. This difference originates

in the difference of forcing since our model obeys the linear mechanism proposed by JM and DF. At high frequency, the more realistic representation of the equatorial dynamics in our model has damped the high frequency oscillations observed in DF.

The mean circulation forced by the wind stress has been neglected in these experiments. We have performed additional experiments which show that this mean circulation does not have a major impact on the results, as already suggested by JM. However, with a second active layer, the Kelvin fronts propagating along the western boundary can interact with the mean circulation in a two gyre system and create anomalies of the thermocline depth at the boundary between the gyres (Février *et al*., 2006).

REFERENCES

Bentsen, M., H. Drange, T. Furevik and T. Zhou. 2004. Simulated variability of the Atlantic meridional overturning circulation. Climate Dyn., *22*, 701–720.

Delworth, T. L. and R. J. Greatbatch. 2000. Multidecadal thermohaline circulation variability driven by atmospheric surface flux forcing. J. Climate, *13*, 1481–1495.

Deshayes, J. and C. Frankignoul. 2005. Spectral characteristics of the response of the meridional overturning circulation to deep water formation. J. Phys. Oceanogr., *35*, 1813–1825.

Février, S., J. Sirven and C. Herbaut. 2006. Interaction of a coastal Kelvin wave with the mean state in the Gulf Stream separation area. J. Phys. Oceanogr., (in press).

Gill, A. E. 1982. Atmosphere-ocean dynamics. Academic Press. 662 pp.

Hakkinen, S. 2001. Variability in sea surface height: a qualitative measure for the meridional over-turning in the North Atlantic. J. Geophys. Res., *106*, 13,837–183,848.

Huang, R. X., M. A. Cane, N. Naik and P. Goodman. 2000. Global adjustment of the thermocline in response to deepwater formation. Geophys. Res. Lett., *27*, 759–762.

Jin, F. F. 1997. A theory of interdecadal climate variability of the north pacific ocean-atmosphere system. J. Climate, *10*, 324–338.

Johnson, H. L. and D. P. Marshall. 2002. A theory for the surface Atlantic response to thermohaline variability. J. Phys. Oceanogr., *32*, 1121–1132.

——— 2004. Global teleconnections of meridional overturning circulation anomalies. J. Phys. Oceanogr., *34*, 1702–1722.

Kawase, M. 1987. Establishment of deep ocean circulation driven by deep-water production. J. Phys. Oceanogr., *17*, 2294–2317.

Kushnir, Y. 1994. Interdecadal variations in North Atlantic sea surface temperature and associated atmospheric conditions. J. Climate, *7*, 141–157.

Marotzke, J. and J. R. Scott. 1999. Convective mixing and the thermohaline circulation. J. Phys. Oceanogr., *29*, 2962–2970.

Pedlosky, J. 1996. Ocean circulation theory. Springer, Berlin, 453 pp.

Primeau, F. 2002. Long Rossby wave basin-crossing time and the resonance of low-frequency basin modes. J. Phys. Oceanogr., *32*, 2652–2665.

Rahmstorf, S. 1995. Multiple convection pattern and thermohaline flow in idealized OGCM. J. Climate, *8*, 3028–3039.

Spall, M. A. 2000. Buoyancy-forced circulations around islands and ridges. J. Mar. Res., *58*, 957–982.

Stommel, H. and A. B. Arons. 1960. On the abyssal circulation of the world ocean—I. Stationary planetary flow patterns on a sphere. Deep-Sea Res., *6*, 140–154.

Timmermann, A. and M. Latif. 1998. Northern hemispheric interdecadal variability: a coupled air-sea mode. J. Climate, *11*, 1906–1931.

Yang J. and J. F. Price. 2000. Water-mass formation and potential vorticity balance in an abyssal ocean circulation. J. Mar. Res., *58*, 789–808.